

MULTILAYER SYSTEM OF LORENTZ/DRUDE TYPE METAMATERIALS WITH DIELECTRIC SLABS AND ITS APPLICATION TO ELECTROMAGNETIC FILTERS

C. Sabah

Physikalisches Institute
Johann Wolfgang Goethe University
Max-von-Laue-Strasse 1, D-60438, Frankfurt am Main, Germany

S. Uckun

Electrical and Electronics Engineering Department
University of Gaziantep
Gaziantep 27310, Turkey

Abstract—In this work, frequency behavior of the multilayer structure comprised of double-negative (DNG) and dielectric slabs is presented in detail. The multilayer structure consists of N pieces DNG and dielectric slabs with different material properties and thicknesses. The incident electric field is assumed to be a monochromatic plane wave with any arbitrary polarization. The DNG layers are realized using the parameters of Lorentz/Drude type metamaterials. Transfer matrix method is used in the analysis to find the characteristics of the reflected and transmitted powers. Finally, the computations of the powers for two structures are demonstrated in numerical results for the application to design efficient filters at the microwave, millimeter wave, and optical frequency regions.

1. INTRODUCTION

Recently, there has been a growing interest on the studies of the double negative (DNG) metamaterials in electromagnetics' community due to the wide potential application of them. The DNG metamaterials have simultaneously negative permittivity and permeability over a certain frequency band and can be constructed artificially to show several exotic properties that cannot be easily achieved using

Corresponding author: C. Sabah (Sabah@Physik.uni-frankfurt.de).

known materials [1–6]. The permittivity and permeability of such metamaterials are realized both analytically and physically by using Lorentz/Drude medium models in various studies [5–28]. Lossy and lossless Lorentz/Drude types of DNG metamaterials are characterized theoretically, used in several experiments, and fabricated for new devices in these studies. For example, wave propagation through the double negative Lorentz/Drude slab embedded between two different dielectric media is studied in [6, 9, 14, 23]. Lorentz types of DNG (LDNG) metamaterials have frequency dispersive parameters, and they can be fabricated using a mixture of conductive spirals or omega particles on printed circuit boards [7, 9, 18]. In addition, they can be manufactured using split ring resonators and wire strips on a circuit board materials [5, 17]. Numerous forms of LDNG metamaterials (also Drude types of DNG (DDNG) metamaterials) can also be found in the literature. Note that this work is considered to be based on the artificial metamaterials which are not similar to the natural metamaterials as in [29] and [30].

In this study, electromagnetic wave interaction with the multilayer media comprised of DNG and dielectric slabs is presented. Theoretically, the multilayer structure is formed from N pieces DNG and dielectric slabs with different material properties and thicknesses. DNG slabs are realized LDNG/DDNG metamaterials. The incident electric field is assumed to be a monochromatic plane wave with any arbitrary polarization. After obtaining the electric and magnetic fields both inside and outside the multilayer structure and imposing the boundary conditions, the incident, reflected, and transmitted powers are determined to observe their features. Although the wave interaction with multilayer DNG media is studied in literature [31–36], the powers and their variations for the structure consisted of DNG (LDNG or DDNG) and dielectric slabs on behalf of the filtering properties have not been investigated yet. Thus, the behavior of the powers for the perpendicular polarization against the frequency is computed and presented in the numerical results.

2. THEORETICAL ANALYSIS

A pair of DNG-dielectric slabs has interesting properties when it is composed as a multilayer structure embedded between two dielectric media. The multilayer structure considered in this paper is composed of N pieces DNG and dielectric layers with different material properties and thicknesses as shown in Figure 1. In this figure, DNG slabs represent LDNG/DDNG metamaterials, and the letter D stands for the conventional dielectric material. We consider any arbitrary

polarization monochromatic plane incident electric field from free-space that is encountering the dielectric-DNG layer interface. In the analysis, $\exp(i\omega t)$ time dependence is assumed and suppressed throughout this work.

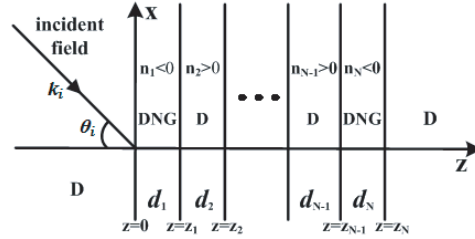


Figure 1. The geometry of multilayer DNG and dielectric slabs.

According to Figure 1, the incident electric field with any arbitrary polarization can be written as follows:

$$\mathbf{E}_i = [E_{i//}(\cos \theta_i \mathbf{a}_x + \sin \theta_i \mathbf{a}_z) + E_{i\perp} \mathbf{a}_y] \cdot \exp[i(k_{ix}x - k_{iz}z)] \quad (1)$$

where θ_i is the angle of the incidence; k_{ix} ($= k_i \sin \theta_i$) and k_{iz} ($= k_i \cos \theta_i$) are the x - and z -components of the wave number k_i ($= \omega \sqrt{\mu_i \varepsilon_i}$). Note that, the subscripts $//$ and \perp refer to the parallel and perpendicular components of the electric field vector, respectively. According to the incident electric field given in Equation (1), the reflected (\mathbf{E}_r) and the transmitted (\mathbf{E}_t) electric fields can be expressed as:

$$\mathbf{E}_r = [E_{r//}(\cos \theta_i \mathbf{a}_x - \sin \theta_i \mathbf{a}_z) + E_{r\perp} \mathbf{a}_y] \cdot \exp[i(k_{ix}x + k_{iz}z)] \quad (2)$$

$$\mathbf{E}_t = [E_{t//}(\cos \theta_t \mathbf{a}_x + \sin \theta_t \mathbf{a}_z) + E_{t\perp} \mathbf{a}_y] \cdot \exp[i(k_{tx}x - k_{tz}z)] \quad (3)$$

where θ_t is the transmission angle; k_t ($= \omega \sqrt{\mu_t \varepsilon_t}$) is the wave number of the transmitted medium; $k_{tx} = k_t \sin \theta_t$ and $k_{tz} = k_t \cos \theta_t$ are the x - and z -components of the wave number k_t .

The electric field in the multilayer structure reflects back and transmits to another stack upon reaching the transmitted medium. Therefore, in the m th slab there are two waves, one propagating toward the right interface and the other propagating toward the left interface. Thus, the total electric field in the m th slab can be stated as:

$$\begin{aligned} \mathbf{E}_m = & [A_{//}(\cos \theta_m \mathbf{a}_x + \sin \theta_m \mathbf{a}_z) + A_{\perp} \mathbf{a}_y] \cdot \exp[i(k_{mx}x - k_{mz}z)] \\ & + [B_{//}(\cos \theta_m \mathbf{a}_x - \sin \theta_m \mathbf{a}_z) + B_{\perp} \mathbf{a}_y] \cdot \exp[i(k_{mx}x + k_{mz}z)] \end{aligned} \quad (4)$$

where $A_{//}$, A_{\perp} , $B_{//}$, and B_{\perp} are the amplitudes of the electric fields inside the m th slab; θ_m is the refracted angle; k_m is the wave number

of the m th slab; $k_{mx} = k_m \sin \theta_m$ and $k_{mz} = k_m \cos \theta_m$ are the x - and z -components of the wave number k_m . Note that, in all representations, the subscripts i , m , and t stand for the incident medium, the m th slab, and the transmitted medium, respectively. If the m th slab is dielectric medium, the wave number k_m must be positive. On the other hand, if the m th slab is DNG medium, the wave number k_m must be negative. Thus, the wave number k_m can be given as:

$$k_m = a\omega\sqrt{\mu_m\varepsilon_m} \quad (5)$$

where $a = +1$ for dielectric slab, $a = -1$ for DNG slab. Note that the permittivity ε_m and the permeability μ_m for the DNG medium are defined using LDNG [3, 5, 12] and DDNG [2, 6, 12] metamaterials which have simultaneously negative permittivity and permeability in a certain frequency band. The permittivity and permeability for the LDNG metamaterial are given as:

$$\varepsilon(\omega) = \varepsilon_o \left(1 - \frac{\omega_{ep}^2 - \omega_{eo}^2}{\omega^2 - \omega_{eo}^2 + j\omega\delta_e} \right) \quad (6)$$

$$\mu(\omega) = \mu_o \left(1 - \frac{\omega_{mp}^2 - \omega_{mo}^2}{\omega^2 - \omega_{mo}^2 + j\omega\delta_m} \right) \quad (7)$$

where ω_{eo} is the electronic resonance frequency; ω_{ep} is the electronic plasma frequency; δ_e is the electronic damping frequency; ω_{mo} is the magnetic resonance frequency; ω_{mp} is the magnetic plasma frequency; and δ_m is the magnetic damping frequency. When $\omega_{eo} = \omega_{mo} = 0$, LDNG metamaterial turns to DDNG metamaterial as:

$$\varepsilon(\omega) = \varepsilon_o \left(1 - \frac{\omega_{ep}^2}{\omega^2 + j\omega\delta_e} \right) \quad (8)$$

$$\mu(\omega) = \mu_o \left(1 - \frac{\omega_{mp}^2}{\omega^2 + j\omega\delta_m} \right) \quad (9)$$

The permittivity and permeability for LDNG and DDNG metamaterials have frequency dependence characteristic, which enable to simultaneously obtain negative permeability and permittivity in a certain frequency range. If these parameters are used in Equation (5), it is seen that the wave number k_m has also frequency dependence characteristic as in the permeability and permittivity.

In order to analyze the multilayer structure shown in Figure 1, it is necessary to impose the boundary conditions at the interfaces of $z = 0$, $z = z_m$ ($m = 1, 2, 3, \dots, N-1$) and $z = z_N$. Consequently, the

relationships among the fields in all regions can be easily obtained by using the transfer matrix method which is skipped here. Details of the using method can be found in [34] and [35].

Now, the tangential components of the incident, reflected, and transmitted powers which are continuous across the boundaries can be represented as follows:

$$\begin{aligned} \mathbf{P}_i &= \mathbf{a}_z \frac{k_{iz}}{2\mu_i} \left| \left(E_{i\perp}^2 + E_{i//}^2 \right) \right|, & \mathbf{P}_r &= \mathbf{a}_z \frac{k_{iz}}{2\mu_i} \left| \left(E_{r\perp}^2 + E_{r//}^2 \right) \right|, \\ \text{and } \mathbf{P}_t &= \mathbf{a}_z \frac{k_{tz}}{2\mu_t} \left| \left(E_{t\perp}^2 + E_{t//}^2 \right) \right| \end{aligned} \quad (10)$$

The conservation of the power for any arbitrary polarization is expressed as:

$$\frac{k_{iz}}{\mu_i} \cdot \left| \left(E_{i\perp}^2 + E_{i//}^2 \right) \right| = \frac{k_{iz}}{\mu_i} \cdot \left| \left(E_{r\perp}^2 + E_{r//}^2 \right) \right| + \frac{k_{tz}}{\mu_t} \cdot \left| \left(E_{t\perp}^2 + E_{t//}^2 \right) \right| \quad (11)$$

3. NUMERICAL RESULTS

In this section, we present the computations for the powers to observe their characteristics using the results obtained in Section 2, when the incident power is normalized to unity. To verify the computations, the conservation of power, as a first method given in Equation (11), is satisfied for all examples. As a second method, a transmission line equivalent is obtained for the structure given in Figure 1 [37]. Both methods give the same numerical values for all computations. Thus, the results are verified by means of two methods. In addition, two structures are considered in numerical results, Structure I (with three layers, $N = 3$) and Structure II (with fifteen layers, $N = 15$). Structure I is in the form of DNG-dielectric-DNG and Structure II is (DNG-dielectric)⁷DNG. Furthermore, the incident electric field is assumed to be a monochromatic plane wave with the perpendicular polarization ($E_{//} = 0$) in all examples. All computations are provided for the normal incidence case ($\theta_i = 0$).

Example I: Here, the reflected (P_r), and transmitted (P_t) powers are calculated as a function of the frequency. The incident and transmitted media are assumed to be free space and glass with $\mu_i = \mu_t = \mu_o$, $\varepsilon_i = \varepsilon_o$, and $\varepsilon_t = 6\varepsilon_o$. The dielectric layers are selected to become silicon dioxide (SiO_2) with $\mu_D = \mu_o$ and $\varepsilon_D = 2.1316\varepsilon_o$. The DNG layers are realized using LDNG metamaterial parameters given in Equations (6) and (7). In the calculations, the following parameters are used as in [3] and [5]: $f_{mp} = 8.50$ GHz, $f_{mo} =$

12.05 GHz, $f_{ep} = 12.80$ GHz, and $f_{eo} = 10.30$ GHz. The operation frequency is selected to be $f_o = 11$ GHz within the frequency band (10.31–12.04 GHz) where the permittivity and permeability of LDNG metamaterial are simultaneously negative. The optical thicknesses are arranged from $|n_{\text{DNG}}d_{\text{DNG}}| = c_1\lambda_o$ and $|n_{\text{D}}d_{\text{D}}| = c_2\lambda_o$ where n_{DNG} and n_{D} are the refractive indices of the related media; c_1 and c_2 are positive real constants; and λ_o is the wavelength in free-space at the operation frequency.

Figure 2 points out the reflected and transmitted powers as a function of the frequency for Structure I. From this plot, when $c_1 = c_2 = 1/4$, the bandwidth extends from 10.31 to 11.5 GHz, and the transmitted power has a sharp peak at 10.86 GHz. At this specific frequency, the structure can be utilized as a band-pass transmission (anti-reflection) filter in which the transmitted power becomes unity, and the reflected power becomes zero. Also, it can be used as a band-stop reflection (anti-transmission) filter in which the powers behave opposite to the previous case. When $c_1 = 1/2$ and $c_2 = 1/4$, it is seen from the dashed lines, the structure behaves like an all-pass filter in a wide range of frequency since the transmitted power is almost constant around one and the reflected power is zero. When $c_1 = 1/4$ and $c_2 = 1/2$, it appears that the reflected and transmitted powers show similar behavior as in dashed lines. But in this case, the frequency range is narrower than the previous one; the transmitted power is around 0.8; and the reflected power is around 0.2 at that range. At this point, it can be said that the multilayer structure forms a high transmission coatings when $c_1 = 1/4$ and $c_2 = 1/2$.

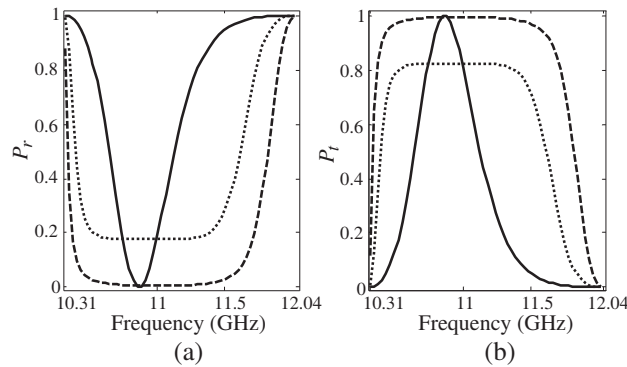


Figure 2. Reflected and transmitted powers as a function of the frequency for Structure I. Solid lines stand for $c_1 = c_2 = 1/4$, dashed lines for $c_1 = 1/2$ and $c_2 = 1/4$, and dotted lines for $c_1 = 1/4$ and $c_2 = 1/2$.

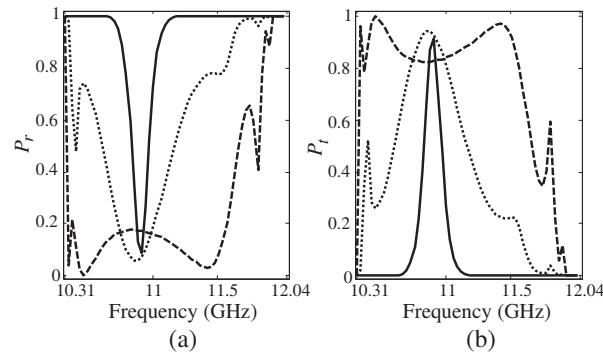


Figure 3. Reflected and transmitted powers as a function of the frequency for Structure II. Solid lines stand for $c_1 = c_2 = 1/4$, dashed lines for $c_1 = 1/2$ and $c_2 = 1/4$, and dotted lines for $c_1 = 1/4$ and $c_2 = 1/2$.

Figure 3 shows the reflected and transmitted powers as a function of the frequency for Structure II. From this figure, the structure can be used as a reflection filter between 10.31–12.04 GHz except for the range 10.7–11.1 GHz when $c_1 = c_2 = 1/4$. Comparing Figure 2 with Figure 3, one can see that the bandwidth where transmitted power has a sharp peak is narrower than that in Structure I. The transmitted power is dominant over a wide range of frequency for $c_1 = 1/2$ and $c_2 = 1/4$. But it is only dominant between the 10.6–11.2 GHz for $c_1 = 1/4$ and $c_2 = 1/2$.

Example II: In this example, we intend to investigate the effect of layer thicknesses on the characteristics of the reflected and transmitted powers. All parameters are the same with Example I except for the thicknesses. Here, the physical thicknesses are used as $d_{\text{DNG}} = c_3 \lambda_0$ and $d_{\text{D}} = c_4 \lambda_0$ where c_3 and c_4 are positive real constants.

Figure 4 displays the frequency response of the reflected and transmitted powers for Structure I. From solid, dashed, and dotted lines, it can be seen that the characteristics of the powers are not smooth here. For all values of c_3 and c_4 , the transmitted power has sharp peaks. Also, it closes to unity at 10.46 GHz when $c_3 = 1/4$ and $c_4 = 1/2$. On the other hand, the reflected power reaches to unity at many frequencies for all cases. In addition, the transmitted power has wide pass bands and narrow stop band regions throughout the frequency spectrum for all cases of c_3 and c_4 . In contrast, the reflected power has narrow pass bands and wide stop band regions.

Figure 5 presents the reflected and transmitted powers versus the frequency for Structure II. As it is seen from this plot, the reflected and transmitted powers are again not smooth as in Figure 4. Pass

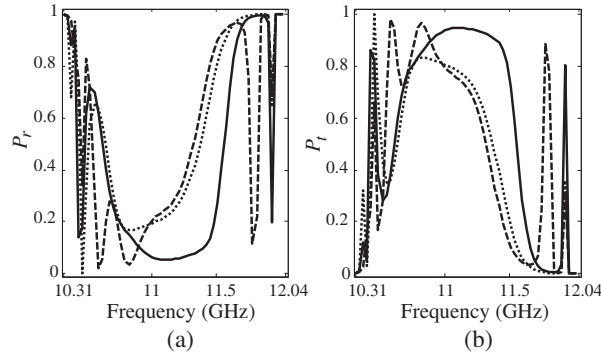


Figure 4. Reflected and transmitted powers versus the frequency for Structure I. Solid lines correspond to $c_3 = c_4 = 1/4$, dashed lines to $c_3 = 1/2$ and $c_4 = 1/4$, and dotted lines to $c_3 = 1/4$ and $c_4 = 1/2$.

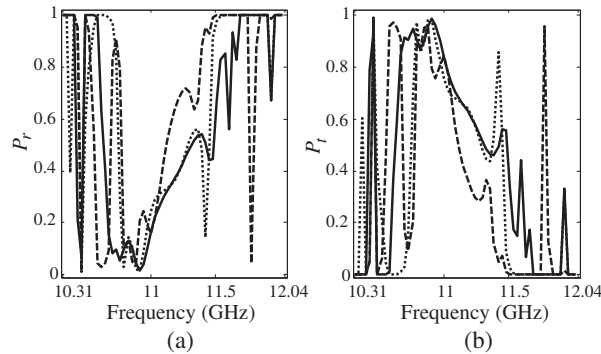


Figure 5. Reflected and transmitted powers versus the frequency for Structure II. Solid lines correspond to $c_3 = c_4 = 1/4$, dashed lines to $c_3 = 1/2$ and $c_4 = 1/4$, and dotted lines to $c_3 = 1/4$ and $c_4 = 1/2$.

band region for the transmitted power is not wide as in the previous figure for all cases of c_3 and c_4 . Also, it has more stop band regions. In return, the reflected power has more pass band and stop band regions for all cases.

According to Figures 4 and 5, two structures act as the band-pass and band-stop filters at some frequency regions. The design of efficient filters can be considered using numerical results obtained here by arranging the structure parameters, layer numbers and thicknesses.

Example III: Here, the DNG layers are realized using DDNG metamaterial parameters given in Equations (8) and (9). In our calculations, the following parameters are used as in [3] and [5]: $f_{mp} =$

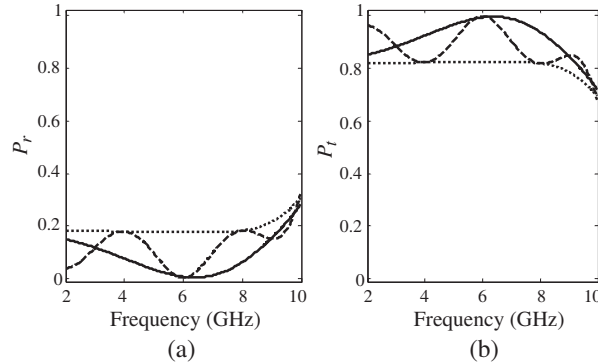


Figure 6. Reflected and transmitted powers against the frequency for Structure I. Solid lines represent $c_1 = c_2 = 1/4$, dashed lines $c_1 = 1/2$ and $c_2 = 1/4$, and dotted lines $c_1 = 1/4$ and $c_2 = 1/2$.

10.95 GHz and $f_{ep} = 14.50$ GHz. The operation frequency is $f_o = 6$ GHz within the frequency band (2–10 GHz) where the permittivity and permeability of DDNG metamaterial are simultaneously negative. The frequency range is wider than the range of LDNG metamaterial. At this point, we can say that the simultaneously negative permittivity and permeability can be realized over a wide frequency band for DDNG metamaterial more easily than for LDNG metamaterial. The thicknesses are again arranged from $|n_{\text{DNG}}d_{\text{DNG}}| = c_1\lambda_o$ and $|n_{\text{D}}d_{\text{D}}| = c_2\lambda_o$. The other parameters are assumed to be the same with the first example.

Figure 6 depicts P_r and P_t against the frequency for Structure I. As it is observed from this plot, $P_r(P_t)$ power shows monotonical decrease (increase) up to 6.5 GHz and then it increases (decreases) with the frequency when $c_1 = c_2 = 1/4$. Full transmission occurs around 6.5 GHz for this case. When $c_1 = 1/2$ and $c_2 = 1/4$, the powers behaves like an oscillatory function up to ~ 8 GHz. Also, they are constant up to this frequency when $c_1 = 1/4$ and $c_2 = 1/2$.

Figure 7 demonstrates P_r and P_t against the frequency for Structure II. The powers do not show monotonical characteristics as in Figure 6 when $c_1 = c_2 = 1/4$. P_t is dominant up to 8.5 GHz in this case. P_r and P_t change periodically between 2–8 GHz when $c_1 = 1/2$ and $c_2 = 1/4$. The powers show slightly periodic behavior when $c_1 = 1/4$ and $c_2 = 1/2$. In the last two cases, P_t is dominant in all frequencies studied here.

From Figures 6 and 7, it can be concluded that, the structure parameters, layer numbers and thicknesses can be arranged to design

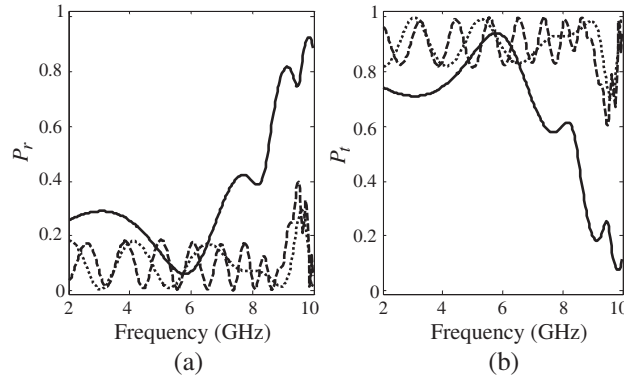


Figure 7. Reflected and transmitted powers against the frequency for Structure II. Solid lines represent $c_1 = c_2 = 1/4$, dashed lines $c_1 = 1/2$ and $c_2 = 1/4$, and dotted lines $c_1 = 1/4$ and $c_2 = 1/2$.

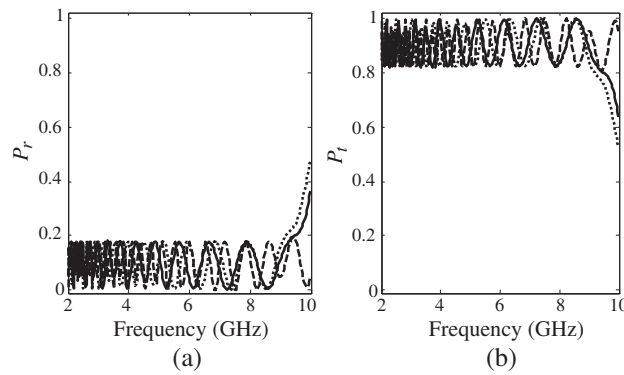


Figure 8. Reflected and transmitted powers against the frequency for Structure I. Solid lines represent $c_3 = c_4 = 1/4$, dashed lines $c_3 = 1/2$ and $c_4 = 1/4$, and dotted lines $c_3 = 1/4$ and $c_4 = 1/2$.

high efficiency transmission filter.

Example IV: In the last example, we present the effect of layer thicknesses on the characteristics of P_r and P_t . All parameters are the same with Example III except for the thicknesses. Here, the thicknesses are $d_{\text{DNG}} = c_3\lambda_o$ and $d_{\text{D}} = c_4\lambda_o$ where c_3 and c_4 are positive real constant.

Figure 8 corresponds to P_r and P_t against the frequency for Structure I. It is seen that P_r oscillates between zero and 0.2 in all cases of c_3 and c_4 . In turn, P_t oscillates between 0.8 and 1.0. P_t is dominant over a wide frequency band in all cases of c_3 and c_4 .

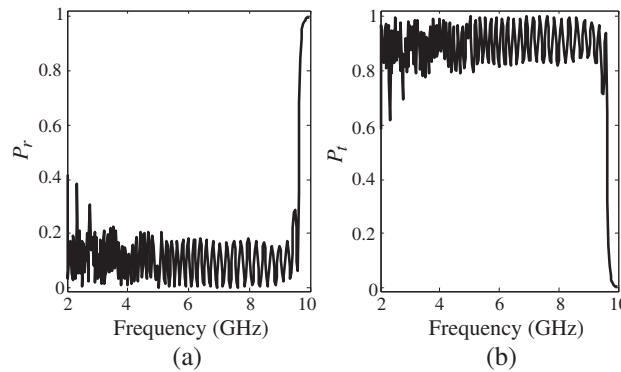


Figure 9. Reflected and transmitted powers against the frequency for Structure II when $c_3 = c_4 = 1/4$.

Figure 9 indicates P_r and P_t against the frequency for Structure II. Only $c_3 = c_4 = 1/4$ case is illustrated in this figure. The other cases are skipped here since P_r and P_t have high oscillating behavior. When $c_3 = c_4 = 1/4$, P_r and P_t show frequent oscillating behavior up to 9.6 GHz. After this frequency P_r increases it becomes unity at 10 GHz. On the other hand, when P_t decreases it becomes zero at 10 GHz.

From Figures 8 and 9, it can be seen that high efficiency oscillating filters for the transmitted wave can be designed by arranging the structure parameters, layer numbers and thicknesses.

It is confirmed that similar numerical results given in Figures 2–9 can be easily obtained for the incident wave with the parallel polarization.

4. SUMMARY AND CONCLUSION

In this paper, frequency behavior of DNG and dielectric multilayers are presented in detail. The multilayer structure is embedded between two dielectric media and the incident electric field is assumed to be plane electromagnetic wave with any arbitrary polarization. The other fields inside and outside the multilayer structure are written using the Maxwell's equations. In this work, the DNG layers are realized using LDNG and DDNG metamaterial parameters in which their properties are given in the analysis. Physically, they can be implemented using artificial materials such as ring resonators, wire medium, etc. Transfer matrix method is used to solve the problem of electromagnetic wave propagation through multilayer structure to obtain the incident, the reflected and the transmitted powers. Finally, the computations of

the powers for two structures are demonstrated in numerical results with the help of home developed simulation code. It can be seen that from the numerical results, the structures given in this study can be utilized as reflection and transmission filters at some frequency band. Specifically, different kinds of electromagnetic filters can be designed for particular applications as desired. Furthermore, the structure transmits most of the incident wave because the transmitted power is dominant over a wide frequency range in some cases. Thus, more capable transmission filters and coatings can be realized in a wide range.

The advantage of this work can be explained as follows: The studied multilayer system has multiple degrees of freedom which enable to easily design and physically perform well-organized and efficient electromagnetic filter structures. This freedom is provided by the optical/physical thicknesses; operation frequency; incidence angle; resonance, plasma, and damping frequencies of the permittivity and permeability (six quantities); layer numbers; and the parameters of incident, dielectric, and transmitted media. The usual systems do not have the additional quantities like resonance, plasma, and damping frequencies. The characteristic features of the filter structures can also be controlled by using these quantities. But, there is no extra possibility to control the properties of structure in the usual systems. This property can open a way to create effective desired constructions. Note that the filtering features can also be obtained via single negative (SNG) materials, and the stop band can be organized by using different SNG layers. However, the studied system has more control parameters than the SNG layers to manage the filter characteristic. Because of the reasons listed above, the DNG (LDNG/DDNG metamaterial) layers are used in our system. In addition, this work can easily be extended to different configurations for filtering applications. Photonic band gap structures may be good candidates for such applications, and they can be considered for future studies.

This work will make a foundation for the future application of the DNG medium using analytical and physical forms of LDNG and DDNG metamaterials. Moreover, it will enable to design band-pass, band-stop, all-pass, and oscillating reflection and transmission filters with high efficiency at the millimeter wave, optical, and microwave regimes.

ACKNOWLEDGMENT

The author would like to thank editors and anonymous reviewers for their suggestions to improve the paper.

REFERENCES

1. Veselago, V. G., "The electrodynamics of substances with simultaneously negative values of ϵ and μ ," *Soviet Physics Uspekhi*, Vol. 10, 509–514, 1968.
2. Pendry, J. B., A. J. Holden, W. J. Stewart, and I. Youngs, "Extremely low frequency plasmons in metallic mesostructures," *Physical Review Letters*, Vol. 76, 4773–4776, 1996.
3. Pendry, J. B., A. J. Holden, D. J. Robbins, and W. J. Stewart, "Magnetism from conductors and enhanced nonlinear phenomena," *IEEE Transactions on Microwave Theory and Techniques*, Vol. 47, 2075–2084, 1999.
4. Smith, D. R., W. J. Padilla, D. C. Vier, S. C. Nemat-Nasser, and S. Schultz, "Composite medium with simultaneously negative permeability and permittivity," *Physical Review Letters*, Vol. 84, 4184–4187, 2000.
5. Shelby, R. A., D. R. Smith, and S. Schultz, "Experimental verification of a negative index of refraction," *Science*, Vol. 292, 77–79, 2001.
6. Ziolkowski, R. W. and E. Heyman, "Wave propagation in media having negative permittivity and permeability," *Physical Review E*, Vol. 64, 056625.1–15, 2001.
7. Tretyakov, S., I. Nefedov, C. Simovski, and S. Maslovski, *Advances in Electromagnetics of Complex Media and Metamaterials*, Kluwer, Dordrecht, MA, 2002.
8. Enoch, S., G. Tayeb, P. Sabouroux, N. Guerin, and P. Vincent, "A metamaterial for directive emission," *Physical Review Letters*, Vol. 89, 213902.1–4, 2002.
9. Karkkainen, M. K., "Numerical study of wave propagation in uniaxially anisotropic Lorentzian backward-wave slabs," *Physical Review E*, Vol. 68, 026602.1–6, 2003.
10. Panoiu, N. C. and R. M. Osgood, Jr., "Numerical investigation of negative refractive index metamaterials at infrared and optical frequencies," *Optics Communications*, Vol. 223, 331–337, 2003.
11. Darmanyan, S. A., M. Neviere, and A. A. Zakhidov, "Surface modes at the interface of conventional and left-handed media," *Optics Communications*, Vol. 225, 233–240, 2003.
12. Cui, T. J. and J. A. Kong, "Time-domain electromagnetic energy in a frequency-dispersive left-handed medium," *Physical Review B*, Vol. 70, 205106.1–7, 2004.
13. Erentok, A., P. L. Luljak, and R. W. Ziolkowski, "Characteriza-

- tion of a volumetric metamaterial realization of an artificial magnetic conductor for antenna applications,” *IEEE Transactions on Antennas and Propagation*, Vol. 1, 160–172, 2005.
14. Engheta, N. and R. W. Ziolkowski, “A positive future for double-negative metamaterials,” *IEEE Transactions on Microwave Theory and Techniques*, Vol. 4, 1535–1556, 2005.
 15. Mirza, I. O., S. Shi, and D. W. Prather, “Calculation of the dispersion diagrams of LHM using the 3D FDTD method,” *Microwave and Optical Technology Letters*, Vol. 45, 394–397, 2005.
 16. Wang, N.-B., Y.-C. Jiao, and F.-S. Zhang, “Analysis of an electrically small cylindrical monopole surrounded by double negative materials using FDTD method,” *Progress In Electromagnetics Research Symposium*, 360, Hangzhou, China, 2005.
 17. Engheta, N. and R. W. Ziolkowski, *Metamaterials — Physics and Engineering Explorations*, IEEE-Wiley Press, Piscataway, NJ, 2006.
 18. Ramadan, O., “An efficient state-space ADI-PML algorithm for truncating DNG metamaterial FDTD domains,” *Microwave and Optical Technology Letters*, Vol. 49, 494–498, 2006.
 19. Zedler, M., C. Caloz, and P. Russer, “3D composite right-left handed metamaterials with Lorentz-type dispersive elements,” *International Symposium on Signals, Systems and Electronics 2007 (ISSSE’07)*, 217–221, Montreal, QC, Canada, 2007.
 20. Linden, S. and M. Wegener, “Photonic metamaterials,” *International Symposium on Signals, Systems and Electronics 2007 (ISSSE’07)*, 147–150, Montreal, QC, Canada, 2007.
 21. Kong, S.-C., Z. M. Thomas, X. Chen, B.-I. Wu, T. M. Grzegorzczak, and J. A. Kong, “Band-stop filter based on a substrate embedded with metamaterials,” *Microwave and Optical Technology Letters*, Vol. 49, 530–534, 2007.
 22. Sabah, C., G. Ögücü, and S. Uckun, “Power analysis of plane waves through a double-negative slab,” *IV. International Workshop on Electromagnetic Wave Scattering — EWS’2006*, 11.61–66, Gebze Institute of Technology, Gebze, Kocaeli, Turkey, 2006.
 23. Sabah, C. and S. Uckun, “Electromagnetic wave propagation through the frequency-dispersive and lossy double-negative slab,” *Opto-Electronics Review*, Vol. 15, 133–143, 2007.
 24. Alu, A., F. Bilotti, N. Engheta, and F. Vegni, “Subwavelength, compact, resonant patch antennas loaded with metamaterials,” *IEEE Transactions on Antennas and Propagation*, Vol. 55, 13–25,

- 2007.
25. Wang, M. Y., J. Xu, J. Wu, Y. Yan, and H. L. Li, "FDTD study on scattering of metallic column covered by double-negative metamaterial," *Journal of Electromagnetic Wave Applications*, Vol. 21, No. 14, 1905–1914, 2007.
 26. Manzanares-Martinez, J. and J. Gaspar-Armenta, "Direct integration of the constitutive relations for modeling dispersive metamaterials using the finite difference time-domain technique," *Journal of Electromagnetic Waves and Applications*, Vol. 21, No. 15, 2297–2310, 2007.
 27. Ekmekci, E. and G. Turhan-Sayan, "Comparative investigation of resonance characteristics and electrical size of the double-sided SRR, BC-SRR and conventional SRR type metamaterials for varying substrate parameters," *Progress In Electromagnetics Research B*, Vol. 12, 35–62, 2009.
 28. Wang, J., S. Qu, H. Ma, J. Hu, Y. Yang, X. Wu, Z. Xu, and M. Hao, "A dielectric resonator-based route to left-handed metamaterials," *Progress In Electromagnetics Research B*, Vol. 13, 133–150, 2009.
 29. Pimenov, A., A. Loidl, K. Gehrke, V. Moshnyaga, and K. Samwer, "Negative refraction observed in a metallic ferromagnet in the gigahertz frequency range," *Physical Review Letters*, Vol. 98, 197401.1–197401.4, 2007.
 30. Kussow, A.-G. and A. Akyurtlu, "Negative refraction index in the magnetic semiconductor $\text{In}_{2-x}\text{Cr}_x\text{O}_3$: Theoretical analysis," *Physical Review B*, Vol. 78, 205202.1–205202.11, 2008.
 31. Kong, J. A., "Electromagnetic wave interaction with stratified negative isotropic media," *Progress In Electromagnetics Research*, PIER 35, 1–52, 2002.
 32. Engheta, N., "Ideas for potential application of metamaterials with negative permittivity and permeability," *Advances in Electromagnetics of Complex Media and Metamaterials*, S. Zouhdi, A. H. Sihvola, and M. Arsalane (eds), 19–37, NATO Science Series, *the Proceedings of NATO Advanced Research Workshop in Marrakech (Bianisotropics'2002)*, Kluwer Academic Publishers, Inc., 2002.
 33. Chew, W. C., "Some reflections on double negative materials," *Progress In Electromagnetics Research*, PIER 51, 1–26, 2005.
 34. Sabah, C. and S. Uckun, "Scattering characteristics of the stratified double-negative stacks using the frequency dispersive cold plasma medium," *Zeitschrift für Naturforschung A*, Vol. 62a, 247–253, 2007.

35. Sabah, C. and S. Uckun, "Physical features of left-handed mirrors in millimeter wave band," *Journal of Optoelectronics and Advanced Materials (JOAM)*, Vol. 9, 2480–2484, 2007.
36. Alu, A. and N. Engheta, "Pairing an epsilon-negative slab with a mu-negative slab: Resonance, tunneling and transparency," *IEEE Transactions on Antennas and Propagation*, Vol. 51, 2558–2571, 2003.
37. Sabah, C., "Analysis, applications, and a novel design of double negative metamaterials," Ph.D. Thesis, Gaziantep University, Gaziantep, Turkey, 2008.